AD-A175 336 VARIATION IN THE AMPLITUDE OF PERTURBATIONS ON THE INNER SURFACE OF AN IM..(U) NAVAL RESEARCH LAB WASHINGTON DC D L BOOK ET AL. 10 NOV 86 NRL-MR-5892 1/1

UNCLASSIFIED F/G 10/1 NL

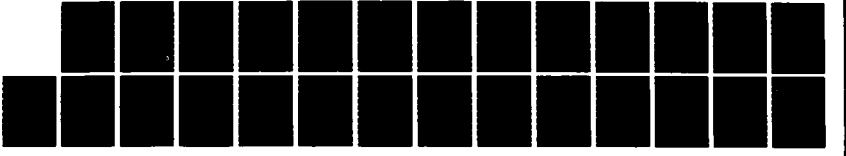

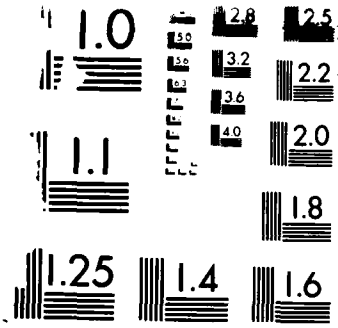

Naval Research Laboratory

Washington, DC 20375-5000 NRL Memorandum Report 5892 November 10, 1986

(2)

Variation in the Amplitude of Perturbations on the Inner Surface of an Imploding Shell During the Coasting Phase

DAVID L. BOOK

Laboratory for Computational Physics

STEPHEN E. BODNER

Laser Plasma Branch
Plasma Physics Division

Approved for public release; distribution unlimited.

SECURITY CLASSIFICATION OF THIS PAGE

REPORT DOCUMENTATION PAGE

1a REPORT SECURITY CLASSIFICATION UNCLASSIFIED	1b RESTRICTIVE MARKINGS
2a SECURITY CLASSIFICATION AUTHORITY	3 DISTRIBUTION/AVAILABILITY OF REPORT Approved for public release; distribution unlimited.
2b DECLASSIFICATION/DOWNGRADING SCHEDULE	
4 PERFORMING ORGANIZATION REPORT NUMBER(S) NRL Memorandum Report 5892	5 MONITORING ORGANIZATION REPORT NUMBER(S)
6a NAME OF PERFORMING ORGANIZATION Naval Research Laboratory 6b OFFICE SYMBOL (If applicable) Code 4040	7a NAME OF MONITORING ORGANIZATION
6c ADDRESS (City, State, and ZIP Code) Washington, DC 20375-5000	7b ADDRESS (City, State, and ZIP Code)
8a NAME OF FUNDING/SPONSORING ORGANIZATION Department of Energy 8b OFFICE SYMBOL (If applicable)	9 PROCUREMENT INSTRUMENT IDENTIFICATION NUMBER
8c ADDRESS (City, State, and ZIP Code) Washington DC 20575	10 SOURCE OF FUNDING NUMBERS PROGRAM ELEMENT NO: PROJECT NO: TASK NO: 81425 WORK UNIT ACCESSION NO: 44-0859-A5

11 TITLE (Include Security Classification)
Variation in the Amplitude of Perturbations on the Inner Surface of an Imploding Shell During the Coasting Phase

12 PERSONAL AUTHOR(S)
Book, David L. and Bodner, Stephen E.

13a TYPE OF REPORT	13b TIME COVERED	14 DATE OF REPORT (Year, Month, Day)	15 PAGE COUNT
Interim	FROM 9/85 TO 6/86	1986 November 10	26

16 SUPPLEMENTARY NOTATION

17 COSATI CODES			18 SUBJECT TERMS (Continue on reverse if necessary and identify by block number)
FIELD	GROUP	SUB-GROUP	
			15

19 ABSTRACT (Continue on reverse if necessary and identify by block number)

In some inertial confinement fusion target designs a spherical shell collapses on a void or compresses a small amount of gaseous material. There can be a period during which both the outside (driver) pressure and the inside pressure have a negligible effect on the implosion dynamics, and the motion is essentially ballistic. The changes in the aspect ratio occur mainly because of geometrical convergence. For reasonable parameters the inner surface does not begin to decelerate until shortly before convergence is complete. We have developed an approximate description of this "coasting" phase and applied it to study the evolution of perturbations on the inner and outer surfaces of the shell in the limit where the fluid is incompressible. The two surfaces are strongly coupled as long as the shell remains thin. When the shell becomes thick compared to the inner radius, the inner and outer surface perturbations decouple. Under these conditions the surface wave action is a good adiabatic invariant, which can be used to estimate the change in the amplitude of a perturbation as a function of the shell inner radius R_1. Detailed analysis confirms the adiabatic invariance argument and extends the results. We speculate that the adiabatic invariant may also be good in the case of compressible fluids.

20 DISTRIBUTION/AVAILABILITY OF ABSTRACT	21 ABSTRACT SECURITY CLASSIFICATION
☒ UNCLASSIFIED UNLIMITED ☐ SAME AS RPT ☐ DTIC USERS	UNCLASSIFIED
22a NAME OF RESPONSIBLE INDIVIDUAL David L. Book	22b TELEPHONE (Include Area Code) (202) 767-3055 / 22c OFFICE SYMBOL Code 4040

DD FORM 1473, 84 MAR 83 APR edition may be used until exhausted
All other editions are obsolete

SECURITY CLASSIFICATION OF THIS PAGE

☆U.S. Government Printing Office 1985—607-047

CONTENTS

VARIATION IN THE AMPLITUDE OF PERTURBATIONS ON THE INNER SURFACE OF AN IMPLODING SHELL DURING THE COASTING PHASE

Introduction

In most inertial fusion target designs the pellet shell goes through three stages during the implosion: acceleration, coasting and deceleration. First the shell is accelerated inward, with Rayleigh-Taylor unstable growth at the outer ablation surface and at any layer interface where a lighter fluid is pushing on a heavier material. Then after the shell reaches nearly its final velocity, it coasts inward with little or no acceleration. With slight oversimplification we can view this phase as ballistic. And finally, the shell decelerates as it compresses the central gas ignitor. This third phase is also Rayleigh-Taylor unstable, on the inner surface of the shell. For a large high-gain pellet, the first phase reduces the pellet radius from about 3000 microns to about 1500 microns. The second phase reduces the radius further to about 150 microns. As the radius decreases tenfold, the mass density and the shell thickness each increase about tenfold. The third phase reduces the radius further to about 75 microns.

During the first (acceleration) phase, Rayleigh-Taylor perturbations on the outer surface drop off radially roughly as $\exp(-lx/R)$, where l is the mode number of the perturbation, R is the shell radius, and x measures the distance inward from the unstable surface. For many mode numbers of interest, the shell is initially so thin that the inner and outer surfaces have about the same perturbation amplitude. These inner-surface pertubations can then serve as a finite-amplitude source for the Rayleigh-Taylor mode during the deceleration phase. The purpose of the present note is to study the evolution of the inner-surface perturbations during the ballistic phase and to examine the role of convergence.

One possibility during the ballistic phase is that the perturbations evolve so that the mass of any protuberance or bulge is conserved. After all, the Rayleigh-Taylor phenomenon moves mass from valleys into bulges. If the Rayleigh-Taylor growth is negligible, one might guess that the mass in a radial sector is conserved according to $\rho R^2 \zeta = \text{const}$, where ζ is the amplitude of an inner-surface perturbation. We find that the perturbations actually evolve quite differently. As the shell thickens and the inner and outer surfaces decouple, "waves" can propagate on the inner surface of the shell. We will show that the action associated with these waves is an adiabatic invariant.

A realistic analytic model would use compressible surface perturbations on a compressible imploding shell. Here, in order to obtain analytically tractable equations, we assume that the perturbations are irrotational and incompressible. This is a plausible assumption, based on other studies of Rayleigh-Taylor instability in compressible and incompressible media. For simplicity we will also assume that the zeroth-order fluid motion is incompressible. This second assumption is not a good one in inertial confinement fusion,

Manuscript approved September 24, 1986

but with this model we can rigorously derive our adiabatic invariant from the fluid equations, study its properties, and gain some physical insight. We suggest that the adiabatic invariant may be useful in the coasting phase even for compressible media.

In order to motivate this approach it is useful to illustrate the physical ideas by means of the example of a pendulum whose length is slowly changing (the "Rayleigh pendulum"). The total energy of a simple pendulum describing small oscillations of amplitude θ in a uniform gravitational field with acceleration g can be written as

$$H = \frac{1}{2}mL^2(\dot{\theta}^2 + g\theta^2/L) = \frac{1}{2}({p_\theta}^2/mL^2 + mgL\theta^2) = \frac{1}{2}mgL\Theta^2, \tag{1}$$

where L is the length, m is the mass, the dot indicates a time derivative, and we have introduced $p_\theta = mL^2\dot{\theta}$, the momentum canonically conjugate to θ. When H is constant the motion of the pendulum is given by $\theta = \Theta \sin \omega(t - t_0)$, where Θ is the amplitude and $\omega = (g/L)^{1/2}$ is the frequency of the oscillations.

If now the gravitational acceleration g, the mass m, or the length L is changed slowly, i.e., over a time Δt such that $\omega \Delta t \gg 1$, then H is no longer conserved but the motion is still approximately harmonic. By a well-known theorem, we can invoke the constancy of the action $\oint p_\theta \, d\theta = \pi m \omega L^2 \Theta^2$, where the integral is carried out over a complete cycle of the motion, to compute the change in Θ. For example, if it is the length which is varied, Θ changes according to $L^{3/2}\Theta^2 = \text{const}$. This result is of course identical with that obtained by direct calculation of the work done on the pendulum by the time-averaged gravitational and centrifugal forces.

On the basis of this example we anticipate that the action of a stable small-amplitude oscillation on the surface of an imploding spherical shell will be a good adiabatic invariant if the implosion time is long compared with the period of the oscillation. From dimensional considerations, we expect the action to be proportional to the product of the square of the perturbation amplitude ζ, the mode frequency ω, and an effective mass. Because the inner surface of a coasting shell accelerates inward on account of convergence effects, waves on the inner surface are stable and satisfy the dispersion relation $\omega \approx (-l\ddot{R}_1/R_1)^{1/2}$, where l is the mode number. If the eigenfunctions satisfy Poisson's equation, they will decay toward the interior of the shell over a characteristic distance of the order of the inverse wavenumber R_1/l. The effective mass will thus be approximately $(4\pi {R_1}^2)(R_1/l)\rho = 4\pi {R_1}^3\rho/l$, and the adiabatic invariant will be

$$4\pi {R_1}^3 \rho \zeta^2 \omega / l \approx \text{const}. \tag{2}$$

Consequently we expect that for a given l the amplitude of a surface perturbation will vary approximately as $(-{R_1}^5\ddot{R}_1)^{-1/4}$.

We begin our investigation by analyzing the motion of a coasting spherical shell. To determine in detail how a surface wave evolves, we then linearize the ideal equations of motion for a shell of uniform density and solve them under the assumption that the flow is incompressible and irrotational. In the following two sections we look at the thin-shell and thick-shell limits. When the shell is thin the perturbations grow linearly in time. For thick shells the perturbations localized on the inner surface decouple from those on the outer. We show that for certain forms of the motion the linearized equations can be solved exactly. In the limit of thick shells and large mode number l we carry out a WKB analysis

of the equation for perturbations on the inner surface and recover the adiabatic invariant (2). To check our analysis we then solve the exact linearized equations numerically. In the last section we discuss these results and offer our conclusions.

Coasting Shell

The total mass and total energy of the imploding shell are conserved. The mass is

$$M = 4\pi \int_{R_1}^{R_2} \rho(R) R^2 \, dR = \frac{4\pi}{3} \bar{\rho} ({R_2}^3 - {R_1}^3) = \frac{4\pi}{3} \bar{\rho} {R_0}^3, \tag{3}$$

where R_1 and R_2 are the inner and outer radii of the shell at time t, $\rho(R)$ is the density as a function of radius, $\bar{\rho}$ is the average density, and R_0 is the radius of the fully collapsed shell. Because the shell is assumed to be incompressible, the volume between R_1 and an intermediate fluid element moving with time-dependent radius R is conserved and we can differentiate to get the velocity $V(R,t)$:

$$R^2 V \equiv R^2 \dot{R} = {R_1}^2 \dot{R}_1. \tag{4}$$

Hence the total energy is

$$\begin{aligned} W &= 2\pi \int_{R_1}^{R_2} \rho(R) \dot{R}^2 R^2 \, dR \\ &\approx 2\pi \bar{\rho} {\dot{R}_1}^2 {R_1}^4 \int_{R_1}^{R_2} \frac{dR}{R^2} = 2\pi \bar{\rho} {\dot{R}_1}^2 {R_1}^3 (1 - R_1/R_2). \end{aligned} \tag{5}$$

For a uniform shell, $\rho(R) = \bar{\rho}$ and Eq. (5) is exact. We assume this in what follows.

The characteristic time associated with the implosion is $(M{R_0}^2/2W)^{1/2}$. It is convenient to choose the zero of time to correspond to $R_1 = 0$. By differentiating Eq. (5) and using Eq. (4) with $R = R_2$ we find the equation of motion of the unperturbed shell,

$$\ddot{R}_1 = \frac{-W}{4\pi\rho {R_1}^4} \left[3 + 2\frac{R_1}{R_2} + \left(\frac{R_1}{R_2} \right)^2 \right]; \tag{6}$$

R_2 satisfies a similar equation. Both are easily solved numerically (Fig. 1). Note that $\ddot{R}_1 < 0 < \ddot{R}_2$, so that perturbations on both surfaces are stable. The quantity in square brackets in Eq. (6) changes by only a factor of two as R_1/R_2 varies between 0 and 1, so to a good approximation we have $\ddot{R}_1 \propto {R_1}^{-4}$, whence $R_1 \propto (-t)^{2/5}$ and

$$\ddot{R}_1/R_1 \propto {R_1}^{-5} \propto (-t)^{-2}. \tag{7}$$

Linearized Equations

For an incompressible fluid the linearized continuity equation can be written

$$\nabla \cdot \mathbf{v} = 0, \tag{8}$$

where $\mathbf{v}$ is the first-order velocity. (Here and throughout this paper, upper-case variables are associated with the unperturbed motion and lower-case variables with the perturbed motion.) If the perturbations are assumed to be irrotational, we can introduce a scalar potential by

$$\mathbf{v} = \nabla\phi. \tag{9}$$

This potential satisfies the Laplace equation,

$$\nabla^2\phi = 0. \tag{10}$$

The solution of Eq. (10) can be written

$$\phi(\mathbf{R},t) = \sum_{l,m}\left[R_1 u_1^{l,m}(t)(R_1/R)^{l+1} + R_2 u_2^{l,m}(t)(R/R_2)^l\right]Y_{l,m}(\theta,\varphi), \tag{11}$$

where u_j, $j = 1,\ 2$, plays the role of a time-dependent amplitude of the velocity perturbation associated with $R = R_j$; $Y_{l,m}$ is the spherical harmonic of order l, m; and the sum is taken over all meridional and zonal mode numbers such that $0 \le |m| \le l < \infty$. Since the perturbed equations are linear, in what follows we specialize to a particular mode and omit the superscripts l, m whenever doing so will cause no confusion.

The velocity associated with this mode is found by taking the gradient of Eq. (11):

$$\begin{aligned}\mathbf{v}(\mathbf{R},t) = \{&u_1(R_1/R)^{l+2}\left[-\hat{\mathbf{e}}_r(l+1)Y_{l,m} + R\nabla Y_{l,m}\right] \\ &+ u_2(R/R_2)^{l-1}\left[\hat{\mathbf{e}}_r l Y_{l,m} + R\nabla Y_{l,m}\right]\},\end{aligned} \tag{12}$$

where $\hat{\mathbf{e}}_r$ is the unit vector in the radial outward direction. The linearized momentum equation can be written

$$\rho\left[\frac{\partial \mathbf{v}}{\partial t} + \nabla(\mathbf{V}\cdot\mathbf{v})\right] + \nabla p = 0. \tag{13}$$

To find the first-order pressure $p(\mathbf{R},t)$ we employ the Bernoulli form of Eq. (13), obtained by combining Eq. (9) with Eq. (13) and integrating:

$$\rho\left(\frac{\partial\phi}{\partial t} + V v_r\right) + p = f(t). \tag{14}$$

The function of t on the right side can be made to vanish by proper choice of ϕ. Substituting Eqs. (11) and (12) in Eq. (14), we obtain

$$\begin{aligned}-\frac{p}{\rho} = \Bigg\{&\left[R_1\dot{u}_1 + (l+2)\dot{R}_1 u_1 - (l+1)\dot{R}_1 u_1\left(\frac{R_1}{R}\right)^3\right]\left(\frac{R_1}{R}\right)^{l+1} \\ &+ \left[R_2\dot{u}_2 - (l-1)\dot{R}_2 u_2 + l\dot{R}_2 u_2\left(\frac{R_2}{R}\right)^3\right]\left(\frac{R}{R_2}\right)^l\Bigg\}Y_{l,m}.\end{aligned} \tag{15}$$

The boundary conditions needed to complete the specification of the problem are the kinematic

$$\dot{\varsigma}_j = v_{rj} + \left(\frac{\partial V}{\partial R}\right)_j \varsigma_j \tag{16}$$

and dynamic

$$p_j + \left(\frac{\partial P}{\partial R}\right)_j \varsigma_j = 0 \tag{17}$$

conditions for $j = 1,\ 2$, where ς_j is the amplitude of the first-order displacement of the jth surface. Equations (16) and (17) are valid regardless of the dynamics of the basic state; i.e., they hold for any form of $R_1(t)$.

Using Eq. (4) and the unperturbed equation of motion in the form

$$\rho\ddot{\mathbf{R}} = -\nabla P, \tag{18}$$

we can rewrite Eqs. (16) and (17) as

$$v_{rj} = \dot{\varsigma}_j + 2\dot{R}_j\varsigma_j/R_j \tag{19}$$

and

$$p_j = \rho\ddot{R}_j\varsigma_j, \tag{20}$$

$j = 1,\ 2$. Setting $R = R_j$ in the radial component of Eq. (12) and substituting the result in (19) yields two linear ordinary differential equations relating ς_1 and ς_2 to u_1 and u_2, which can be written as

$$\dot{\varsigma}_1 + 2(\dot{R}_1/R_1)\varsigma_1 = -(l+1)u_1 + lA^{l-1}u_2 \tag{21}$$

and

$$\dot{\varsigma}_2 + 2(\dot{R}_2/R_2)\varsigma_2 = -(l+1)A^{l+2}u_1 + lu_2, \tag{22}$$

where $A = R_1/R_2$. Combining Eq. (15) with Eq. (20), we have

$$(R_1u_1)^{\cdot} + \left\{R_2\dot{u}_2 + \left[lA^{-3} - l + 1\right]\dot{R}_2u_2\right\}A^l = -\ddot{R}_1\varsigma_1 \tag{23}$$

and

$$\left\{R_1\dot{u}_1 + \left[l + 2 - (l+1)A^3\right]\dot{R}_1u_1\right\}A^{l+1} + (R_2u_2)^{\cdot} = -\ddot{R}_2\varsigma_2. \tag{24}$$

Equations (21)–(24) constitute a fourth-order system of linear ordinary differential equations in ς_1, ς_2, u_1, and u_2. Before solving them numerically we analyze them in the limits in which the shell is thin or thick compared with the radius.

Thin-Shell Limit

When the shell thickness $r = R_2 - R_1$ is much less than either R_1 or R_2, we have to a good approximation

$$\frac{r}{R} = \frac{R_0^3}{3R^3}, \tag{25}$$

where $R = \frac{1}{2}(R_1 + R_2)$. Hence we can expand the perturbation amplitudes $\varsigma_j = \varsigma_j^0 + \varsigma_j^1$ and the coefficients in the velocity potential $u_j = u_j^0 + u_j^1$, $j = 1, 2$, where

$$\varsigma_j^1/\varsigma_j^0 \sim u_j^1/u_j^0 \sim r/R \ll 1. \tag{26}$$

By Eq. (6) and its analog for R_2 the accelerations $\ddot{R}_j$ are first-order quantitities, so to lowest order Eqs. (23) and (24) both yield

$$\left[R(u_1^0 + u_2^0)\right]^{\cdot} = 0, \tag{27}$$

whence we obtain

$$u_2^0 = -u_1^0 + C/R, \tag{28}$$

where C is constant. Hence Eqs. (21) and (22) in lowest order become

$$\dot{\varsigma}_1^0 + 2\frac{\dot{R}}{R}\varsigma_1^0 = -(2l+1)u_1^0 + \frac{lC}{R} \tag{29}$$

and

$$\dot{\varsigma}_2^0 + 2\frac{\dot{R}}{R}\varsigma_2^0 = (2l+1)u_2^0 - \frac{(l+1)C}{R}. \tag{30}$$

In first order Eqs. (23) and (24) yield

$$\left[R(u_1^1 + u_2^1)\right]^{\cdot} - \frac{1}{2}(ru_1^0)^{\cdot} + \frac{1}{2}(ru_2^0)^{\cdot} - \frac{lr}{R}\left[(Ru_2^0)^{\cdot} - 3\dot{R}u_2^0\right] = \frac{3W\varsigma_1^0}{2\pi\rho R^4} \tag{31}$$

and

$$\left[R(u_1^1 + u_2^1)\right]^{\cdot} - \frac{1}{2}(ru_1^0)^{\cdot} + \frac{1}{2}(ru_2^0)^{\cdot} - \frac{(l+1)r}{R}\left[(Ru_1^0)^{\cdot} - 3\dot{R}u_1^0\right] = -\frac{3W\varsigma_1^0}{2\pi\rho R^4}. \tag{32}$$

Subtracting Eq. (32) from Eq. (31), we obtain

$$(2l+1)\left[r\dot{u}_1^0 - 2\frac{\dot{R}}{R}ru_1^0\right] = \frac{3W\varsigma_1^0}{\pi\rho R^4} - \frac{3lC\dot{R}r}{\pi\rho R^2}. \tag{33}$$

Differentiating Eq. (25) twice with respect to t, we find that $\dot{r} = -2(\dot{R}/R)r$ and $\ddot{r} = 6(\dot{R}/R)^2 r$. If we multiply Eq. (29) by r, differentiate, substitute Eq. (33) in the right-hand side, and use the expressions for r and its derivatives, we find that ς_1^0 satisfies

$$\ddot{\varsigma}_1^0 = \left(\frac{6\dot{R}^2}{R^2} - \frac{9W}{\pi\rho {R_0}^3 R^2}\right)\varsigma_1^0 = 0, \tag{34}$$

where we have used the thin-shell limit of Eq. (5). Going through similar operations using Eq. (30) instead of Eq. (29), we find that the second derivative of ς_2^0 likewise vanishes. Thus both ς_1 and ς_2 vary linearly with time. This simple result should come as no surprise: when the unperturbed motion of the shell is uniform, so is that of the perturbations.

Thick-Shell Limit

Equations (21)–(24) also simplify considerably in the thick-shell limit. If $A^l \ll 1$, the perturbations localized on the inner and outer surfaces decouple and satisfy

$$\frac{d}{dt}\left[\frac{1}{R_1}\frac{d}{dt}\left({R_1}^2\zeta_1\right)\right] = (l+1)\ddot{R}_1\zeta_1 \tag{35}$$

and

$$\frac{d}{dt}\left[\frac{1}{R_2}\frac{d}{dt}\left({R_2}^2\zeta_2\right)\right] = -l\ddot{R}_2\zeta_2, \tag{36}$$

respectively. We are particularly interested in the behavior of the former. Here we discuss several examples for which Eq. (35) can be solved exactly.

(*i*) *Coasting shell.* If we substitute Eq. (7) in Eq. (35), we find that $\zeta_1 \propto (-t)^\alpha$, where

$$\alpha = -\frac{1}{10} \pm \frac{1}{10}\sqrt{25-24l}. \tag{37}$$

For $l > 1$, α is complex with real part equal to $-1/10$. Hence as $t \to 0$, we have $|\zeta_1| \sim (-t)^{-1/10} \sim {R_1}^{-1/4}$ by Eq. (7). This divergence is much weaker than that ($\sim {R_1}^{-2}$) predicted by the "constant-mass perturbation" model.

(*ii*) *Constant acceleration.* The linearized equations derived above hold for any $R_1(t)$, even one which does not conserve the energy of the unperturbed state. If the shell undergoes constant acceleration $G < 0$ and reaches the origin at $t = 0$ with velocity $U < 0$, then its radius as a function of time is given by

$$R_1(t) = \tfrac{1}{2}Gt^2 + Ut. \tag{38}$$

Evidently V_1 vanishes and R_1 attains its maximum at $t_0 = -U/G$. Equation (35) becomes

$$(\tfrac{1}{2}Gt^2 + Ut)\ddot{\zeta}_1 + 3(Gt+U)\dot{\zeta}_1 - (l-1)G\zeta_1 = 0. \tag{39}$$

If we set $x = -Gt/2U$, then $z = \zeta_1$ satisfies the hypergeometric equation[1]

$$x(1-x)z'' + [c - (a+b+1)x]z' - abz = 0, \tag{40}$$

$0 \le x \le \frac{1}{2}$, where primes denote differentiation with respect to x and

$$a = \tfrac{1}{2}(5 + \sqrt{17+8l}); \tag{41a}$$

$$b = \tfrac{1}{2}(5 - \sqrt{17+8l}); \tag{41b}$$

$$c = 3. \tag{41c}$$

One solution of Eq. (40) is the hypergeometric function $z_1 = F(a,b;c;x)$, which equals unity at $x = 0$ and takes on the value $2\sqrt{\pi}\left[\Gamma(\frac{1}{2}a+\frac{1}{2})\Gamma(\frac{1}{2}b+\frac{1}{2})\right]^{-1}$ at $x = 1/2$. Since z_1 is related to the associated Legendre functions by[1]

$$F\left[a,b;\tfrac{1}{2}(a+b+1);x\right] = \Gamma\left[\tfrac{1}{2}(a+b+1)\right][x(1-x)]^{\frac{1}{2}(1-a-b)}P^{\frac{1}{2}(1-a-b)}_{\frac{1}{2}(a-b-1)}(1-2x), \tag{42}$$

the series for z_1 reduces to a polynomial in x when $(17+8l)^{1/2}$ is an odd integer, i.e., for $l = 1, 4, 8, 13, \ldots$. The second solution z_2 is finite at $x = 1/2$ but diverges at $x = 0$ as $z_2 \sim x^{-2} \sim (-t)^{-2}$. This suggests that the growth of the inner surface perturbations is more serious for an accelerated shell than for one which coasts.

(*iii*) *Simple harmonic motion.* If the shell radius varies with time according to

$$R_1(t) = \tilde{R}_1 \sin(-\Omega_0 t), \tag{43}$$

where $\tilde{R}_1$ and Ω_0 are constant, then we can set $x = \sin^2 \Omega_0 t$ and again arrive at Eq. (40), with

$$a = \tfrac{1}{4}(3 + \sqrt{5+4l}); \tag{44a}$$

$$b = \tfrac{1}{4}(3 - \sqrt{5+4l}); \tag{44b}$$

$$c = 2. \tag{44c}$$

The two solutions behave similarly to those found in case (*ii*): z_1 is finite for $0 \le x \le 1$ and reduces to a polynomial in x if $(5+4l)^{1/2}$ is an odd integer, i.e., for $l = 1, 5, 11, 19, \ldots$; z_2 diverges at $t = 0$ as $1/x \sim (-t)^{-2}$.

(*iv*) *Mode number* $l = 1$. For $l = 1$ Eq. (35) becomes

$$R_1 \ddot{\zeta}_1 + 3\dot{R}_1 \dot{\zeta}_1 = 0, \tag{45}$$

which has two types of solutions, satisfying

$$\zeta_1 = \text{const} \tag{46}$$

and

$$R_1{}^3 \dot{\zeta}_1 = \text{const}, \tag{47}$$

respectively. For a thick coasting shell, when $R_1 \ll R_2$, Eq. (47) can be rewritten using Eq. (5) as

$$R_1{}^{3/2} \frac{d\zeta_1}{dR_1} \approx \text{const}, \tag{48}$$

which implies

$$R_1{}^{1/2} \zeta_1 \approx \text{const}. \tag{49}$$

In general $\zeta_1(t)$ is a superposition of these two solutions. The second one blows up as $R_1 \to 0$, however, and therefore dominates for sufficiently small R_1. Consequently we expect ζ_1 to diverge as $R_1{}^{-1/2}$ in this limit. However, as is well known, this apparent divergence is merely a shift in the location of the origin.

WKB Analysis for Thick Shells

We look for a rapidly oscillating solution to Eq. (35) in the form

$$\varsigma_1(t) = z(t) \exp\left[i \int_0^t \omega(t')\, dt'\right], \tag{50}$$

where the argument of the exponential is assumed large compared with unity (the WKB or quasiclassical approximation). Substituting in Eq. (35), we obtain

$$-\omega^2 R_1 z + i(3\omega \dot{R}_1 z + 2\omega R_1 \dot{z} + \dot{\omega} R_1 z) + R_1 \ddot{z} + 3\dot{R}_1 \dot{z} + 2\ddot{R}_1 z = (l+1)\ddot{R}_1 z. \tag{51}$$

In lowest order we find an expression for the square of the mode frequency,

$$\omega^2(t) = -(l+1)\ddot{R}_1/R_1. \tag{52}$$

Evidently the approximation is good when $l \gg 1$. In next order we have

$$3\omega \dot{R}_1 z + 2\omega R_1 \dot{z} + \dot{\omega} R_1 z = 0, \tag{53}$$

whence

$$R_1^3 z^2 \omega = \text{const.} \tag{54}$$

This is nothing other than the adiabatic invariant (2). It is interesting to note that when $R_1 \propto (-t)^{2/5}$ (the form which holds for a coasting shell), Eq. (54) predicts that the amplitude of the perturbation varies as $(R_1)^{-1/4}$, the exact answer found in example (i) above.

The result (54) can be reached by another, slightly different, approach. In the thick-shell limit, the total kinetic energy associated with the part of the perturbation (11) localized at the inner surface can be represented as

$$W_K = \iiint d^3R\, \tfrac{1}{2}\rho v^2 = \sum_{l,m} W_K^{l,m}, \tag{55}$$

where

$$\begin{aligned} W_K^{l,m} &= \frac{1}{2}\rho \int_{R_1}^{\infty} dR\, R^2 \left(\frac{R_1}{R}\right)^{2l+4} u_1^{l,m} (u_1^{l,m})^* \\ &\qquad \iint d\Omega \left[-\hat{\mathbf{e}}_r (l+1) Y_{l,m} + R\nabla Y_{l,m}\right] \cdot \left[-\hat{\mathbf{e}}_r (l+1) Y_{l,m} + R\nabla Y_{l,m}\right]^* \\ &= \frac{\rho {R_1}^3 \left|u_1^{l,m}\right|^2}{2(2l+1)} \iint d\Omega \left[(l+1)^2 |Y_{l,m}|^2 + R^2 |\nabla Y_{l,m}|^2\right] \\ &= 2\pi\rho {R_1}^3 \frac{(l+1)\left|u_1^{l,m}\right|^2}{2l+1}, \end{aligned} \tag{56}$$

where $d\Omega$ is the differential of solid angle and we have used the fact that v is real; the asterisk (*) denotes complex conjugation. The effective gravitational energy of the perturbation due to the inward acceleration of the shell can be expressed as

$$\begin{aligned} W_G &= -\rho {R_1}^2 \ddot{R}_1 \iint d\Omega \int_0^{\varsigma_1} d\varsigma\, \varsigma \\ &= -\frac{1}{2}\rho {R_1}^2 \ddot{R}_1 \iint d\Omega\, {\varsigma_1}^2 \\ &= -\frac{1}{2}\rho {R_1}^2 \ddot{R}_1 \sum_{l,m} \left|\varsigma_1^{l,m}\right|^2 \iint d\Omega\, |Y_{l,m}|^2 \\ &= -2\pi\rho {R_1}^2 \ddot{R}_1 \sum_{l,m} \frac{\left|\varsigma_1^{l,m}\right|^2}{2l+1} \equiv \sum_{l,m} W_G^{l,m}. \end{aligned} \tag{57}$$

[In Eqs. (56) and (57) we have restored the superscripts l, m labeling the coefficients $u_1^{l,m}$ and $\varsigma_1^{l,m}$ in the summations.] Combining these expressions, we see that the total energy associated with the perturbation can be expressed as a sum over all mode numbers of the energy $W^{l,m} = W_K^{l,m} + W_G^{l,m}$ associated with each (l, m) mode. Here

$$\begin{aligned} W^{l,m} &= \frac{2\pi\rho {R_1}^3}{2l+1}\left\{(l+1)\left|u_1^{l,m}\right|^2 - \frac{\ddot{R}_1}{R_1}\left|\varsigma_1^{l,m}\right|^2\right\} \\ &= \frac{2\pi\rho {R_1}^3}{(l+1)(2l+1)}\left\{\left|\frac{1}{{R_1}^2}\frac{d}{dt}\left({R_1}^2\varsigma_1^{l,m}\right)\right|^2 - \frac{(l+1)\ddot{R}_1}{R_1}\left|\varsigma_1^{l,m}\right|^2\right\} \\ &= \mu\left[\dot{q}_{l,m}\dot{q}^*_{l,m} - \frac{(l+1)\ddot{R}_1}{R_1} q_{l,m} q^*_{l,m}\right], \end{aligned} \tag{58}$$

where $\mu = 2\pi\rho/(l+1)(2l+1)R_1$, $q_{l,m} = {R_1}^2\varsigma_1^{l,m}$, and we have used Eq. (21) in the thick-shell limit $A \to 0$ to replace $u_1^{l,m}$ with an expression involving $\varsigma_1^{l,m}$.

Equation (58) can be put in Hamiltonian form. The momenta canonically conjugate to $q_{l,m}$ are defined by $p_{l,m} = \mu\dot{q}^*_{l,m}$ for all l, m. With this substitution, Eq. (58) becomes

$$W^{l,m} = \mu^{-1} p_{l,m} p^*_{l,m} + {\omega_l}^2 q_{l,m} q^*_{l,m}, \tag{59}$$

where ${\omega_l}^2 = -(l+1)\ddot{R}_1/R_1$. Equation (35), Hamilton's equation of motion for $q_{l,m}$, follows directly from Eq. (59). The adiabatic invariant (54), which is essentially $\oint p_{l,m}\, dq_{l,m}$, also follows from Eq. (59) by the same theorem used earlier to calculate the adiabatic invariant for the simple pendulum. (In fact the two Hamiltonians are formally almost identical.)

Numerical Solution

Equations (21)–(24) can be solved numerically for arbitrary functions $R_1(t), R_2(t)$. For each choice of the basic state, each value of the mode number l in general gives rise to four independent solutions. An exhaustive survey of the behavior of surface perturbations is thus clearly impractical. Instead, we limit ourselves to studying the evolution of a representative sample of the solutions corresponding to a single choice of basic state: the coasting shell which served as the original focus for this investigation.

We suppose that the shell enters the coasting phase with small imperfections, possibly as a result of instabilities which developed during the ablative drive stage. Since the shell is very thin, these irregularities are likely to take the form of "wrinkles," i.e., ripples which do not alter the shell thickness, so we set $\zeta_1 = \zeta_2$. We can assume that they are initially quasistatic, so that $u_1 = u_2 = 0$. Since the perturbed equations are linear, we can Fourier-analyze and set the initial amplitudes of each mode equal to unity without loss of generality. We follow the evolution of ten different harmonics, with mode numbers given by 1, 2, 5, 10, 20, 50, 100, 200, 500, and 1000. The initial velocity (or energy) of the shell determines the time scale of both perturbed and unperturbed equations; thus the only free parameter in the problem is the initial shell inner radius $R_1(t_0)$. By taking this to be very large compared with R_0, the radius of the sphere which results when the shell collapses completely, we can ensure that the solutions depend on this choice only trivially.

Our numerical results were obtained on a VAX 11/780. The unperturbed and perturbed equations were advanced simultaneously using a fourth-order Runge-Kutta-Gill scheme. In our numerical solution we retained the convention adopted in Fig. 1, according to which radial distances are measured in units of R_0 and times in units of R_0 divided by the initial shell speed. We took the initial value of the shell inner radius to be equal to 100, corresponding to an initial time $t_0 = -99.28$. This means that, by Eq. (25), the ratio of the shell thickness to the radius is $r/R \approx 3 \times 10^{-7}$. This is the amount by which the ratio A of the shell surface radii differs from unity. Since the determinant of $\dot{u}_1$ and $\dot{u}_2$ in Eqs. (23)–(24) equals $1 - A^{2l+1}$, the equations are poorly conditioned initially, and it was necessary to solve them in double precision (52-bit mantissas). The time step was chosen to be $\delta t = 0.01 R_1/|\dot{R}_1|$; with this choice R_1 decreased by a factor of 10^5 in 1140 timesteps. By any realistic standard, five orders of magnitude is an enormous radial compression. The reason for doing this was to include in the example both the thin- and the thick-shell regimes, and to make sure that the choice of initial radius did not play an excessively large role. The accuracy of the calculation was monitored by checking conservation of mass and energy and by comparing the numerical results with those obtained analytically. Refining δt by a factor of 2 produced a negligible change in the results. Most of the variation in the solutions takes place where R_1 deviates significantly from linear dependence on t, between $t = -1$ and $t = 0$ [Fig. 1(*b*)], so we plotted all results against $\log R_1$ instead of t or R_1.

Figure 2 shows plots of $(R_1/R_2)^l$ as a function of $\log R_1$ for the ten values of l used. If the transition from "thin" to "thick" is defined to occur when $(R_1/R_2)^l = 0.5$, then we can approximate the transition radius by

$$R_1^{\rm tr} \approx 0.4\, l^{0.4}. \tag{60}$$

Figure 3 displays the linear growth (which appears curved because of the logarithmic scale of the abscissa) predicted by the thin-shell approximation. In Fig. 4 the amplitude of the

perturbation on the inner surface obtained from the adiabatic invariant (54) is plotted, also normalized to unity at $R_1 = 100$. Note that it describes amplification by slightly more than a factor of twenty over the range of the calculation. As can be seen, the thin-shell and the thick-shell approximations cross near $R_1 = 1.25$, i.e., in the middle of the range of the transition radii defined by Eq. (60).

Figures 5(a) and 5(b), respectively, show ζ_1 and ζ_2 as functions of R_1 for $l = 1$. Note that the two amplitudes behave very differently: ζ_1 grows monotonically, while ζ_2 reaches a maximum of 2.9, then approaches unity (the initial value) as $R_1 \to 0$. The dashed curve on Fig. 5(a) represents the approximation (49) with the constant set equal to 11.2. As can be seen, it is reasonably close to the exact solution throughout the range $10^{-3} < R_1 < 100$.

Figure 6 displays the time dependence of the calculated values of the perturbation amplitudes. Note that the amplitudes for the inner (solid trace) and outer (broken trace) coincide and follow the thin-shell approximation shown in Fig. 3 until $R_1 \approx R_1^{\rm tr}$. As $R_1 \to 0$ we see that ζ_1 diverges while oscillating as a function of $\log R_1$ with a frequency that scales roughly as $l^{1/2}$; in contrast, ζ_2 approaches a finite value of order unity. Perhaps the most significant fact that emerges from these results is that ζ_1 grows by a factor of about twenty while R_1 is changing by five orders of magnitude.

To compare this behavior with the prediction obtained from the conservation of action, which is expected to work best in this limit, we have replotted ζ_1 in Fig. 7, scaled by the amplitude $\zeta_1^{\rm ad}$ shown in Fig. 4. It is clear that the adiabatic invariant does an extremely good job of predicting the envelope of the oscillations for all $l > 1$. Not only is the envelope of the rescaled amplitude nearly constant through the last three decades of variation of R_1, but the constant value, which is approximately equal to unity, is almost independent of l. Except for the $l = 1$ case (which corresponds merely to displacement of the shell center without deformation), the thin-shell approximation and the adiabatic invariant between them thus describe essentially the whole evolution of the linear perturbations.

Conclusions

The constant-mass perturbation model predicts that when R_1 decreases by a factor of 10^5, ζ_1 increases by $\sim 10^{10}$. This estimate, which is based on simple geometric considerations, omits the dynamical effects in the problem. It is equivalent to setting the terms on the right hand side of Eq. (21) to zero. Our model predicts amplification by a factor of approximately 20. Evidently the terms on the right hand side of Eq. (21), though initially small, play an important role in reducing the growth of the perturbations. In view of the idealizations in our model and of the many assumptions it incorporates, the coasting approximation is unlikely to be good over a time during which R_1 changes by more than 10 or 100 and the perturbation amplitude increases by a factor of two to three. Hence our quantitative results should be regarded as being merely indicative.

The results of our numerical example suggest that conservation of action is an extremely reliable tool for predicting the evolution of surface waves on an imploding spherical shell. Although these results are strictly applicable only to a model in which the shell is uniform, incompressible, and coasting, the adiabatic invariant (54) can probably be used to describe incompressible irrotational perturbations whenever $\ddot{R}_1 < 0$ and the shell is "thick." Note that even though the waves undergo amplification, we are not talking here about an instability, such as the Rayleigh-Taylor instability. The imploding shell is stable

against Rayleigh-Taylor modes; in fact, if the sign of $\tilde{R}_1$ were reversed, the present theory would no longer hold.

The formalism which gave rise to Eqs. (21)–(24) can probably be generalized in a number of ways. First, the shell could be made up of several uniform layers, or even vary as $\exp\left[\beta(R^3 - {R_1}^3)\right]$, where $\beta = \text{const}$, and still be consistent with Eq. (4). Second, the requirement of irrotationality could be relaxed. Third, it is conceivable that additional physical processes could be modeled, e.g., loss of material through ablation. The requirement that the basic state be incompressible is essential, however; otherwise the unperturbed motion of the shell would be much more complicated because the pressure buildup associated with convergence would cause large-amplitude sound waves to propagate radially through it. In spite of this it is plausible that incompressible surface perturbations on a compressible shell are accurately described by Eq. (54). This assertion is supported by comparison of the behavior of the unstable case (the Rayleigh-Taylor instability) in compressible and incompressible media. It has been shown[2], e.g., that compressibility changes growth rates by a less than a factor of two.

In summary:

(*i*) We have defined the "coasting state" of an imploding spherical shell and derived an analytical description of its behavior.

(*ii*) We have derived a formalism for describing the evolution of infinitesimal irrotational perturbations of an incompressible uniform imploding spherical shell.

(*iii*) We have obtained the limiting form of these equations for the cases of a thin shell and a thick shell, and have exhibited several analytical solutions for the latter.

(*iv*) We have recovered the law of conservation of wave action from the equation for the evolution of a surface wave on the inner surface of a thick shell.

(*v*) We have numerically solved the exact equations for the evolution of the coupled inner and outer surface waves and shown that they are accurately approximated by the solutions in the thin- and thick-shell limits.

(*vi*) We find that for realistic compression factors, perturbations of the inner surface are amplified very little, by only a factor of order two or three. This shows the inadequacy of the simple picture in which the mass of a bump or asymmetry per unit solid angle is conserved.

Acknowledgment

We wish to thank Prof. I. B. Bernstein for a useful discussion. This work was supported in part by the U.S. Dept. of Energy.

References

1. F. Oberhettinger, "Hypergeometric Functions," in M. Abramowitz and I. A Stegun (Eds.), *Handbook of Mathematical Functions*, Dover, New York (1965).

2. D. L. Book, "Rayleigh-Taylor Instability in Compressible Media," in N. P. Cheremisinoff (Ed.), *Encyclopedia of Fluid Mechanics*, Vol. 1, Gulf Publishing Co., Houston (1986).

3. D. L. Book, "Acoustic Amplification in Imploding Spherical Shells," *Phys. Rev. Lett.* **41**, 1551 (1978).

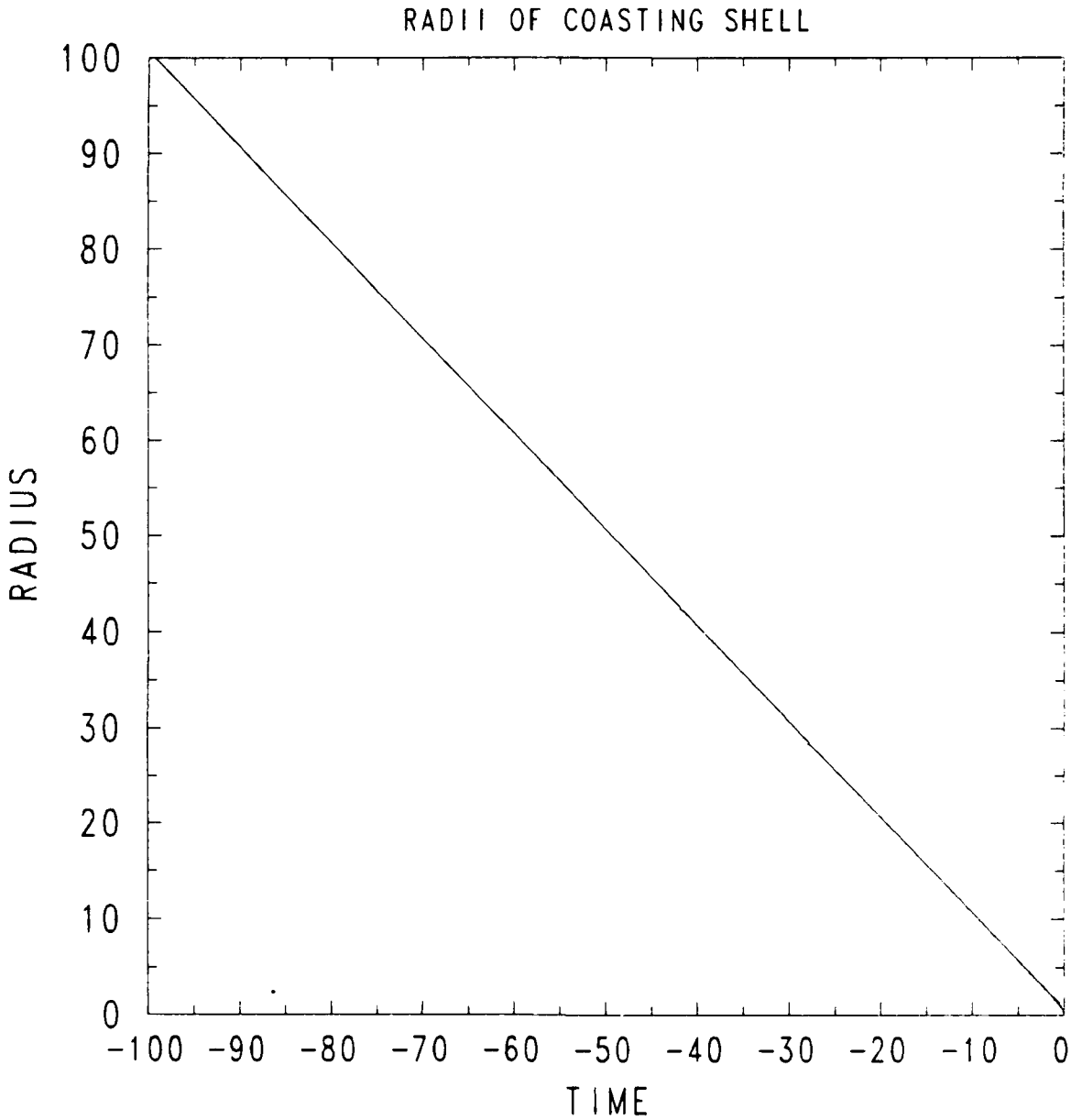

Fig. 1(a) Time histories of R_1 and R_2 for a coasting shell. (The two traces are indistinguishable on this scale). The initial position and velocity of the shell are $R_1 = 100.0$ and $V_1 = -1.0$, respectively, and the zero of time is chosen at the point when $R_1 = 0.0$ and $R_2 = R_0$ ($= 1.0$ in these units).

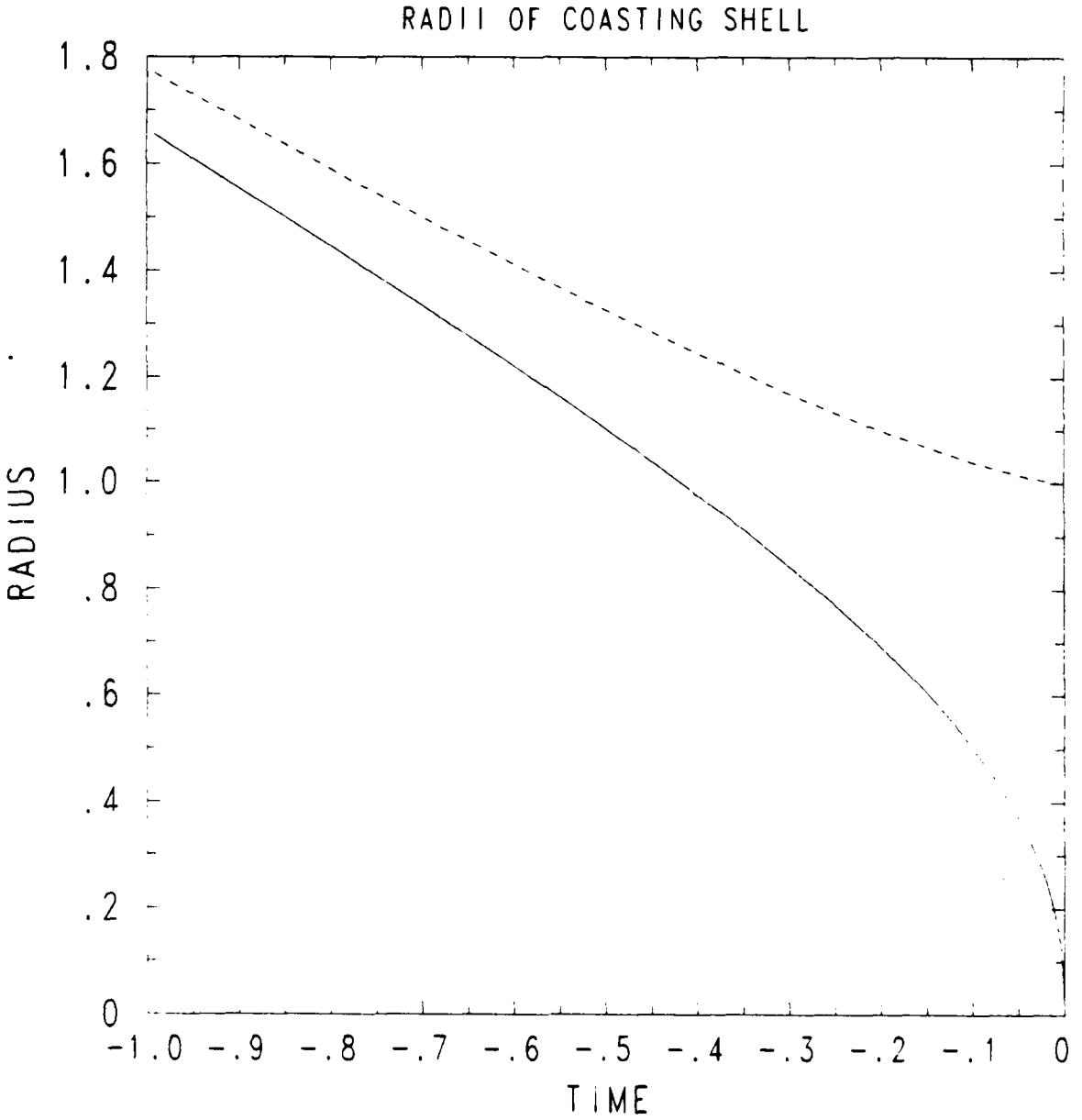

Fig. 1(b) Blowup of traces of R_1 and R_2 vs t for $-1.0 < t < 0$. The inner radius is represented by the solid line, the outer by the broken line.

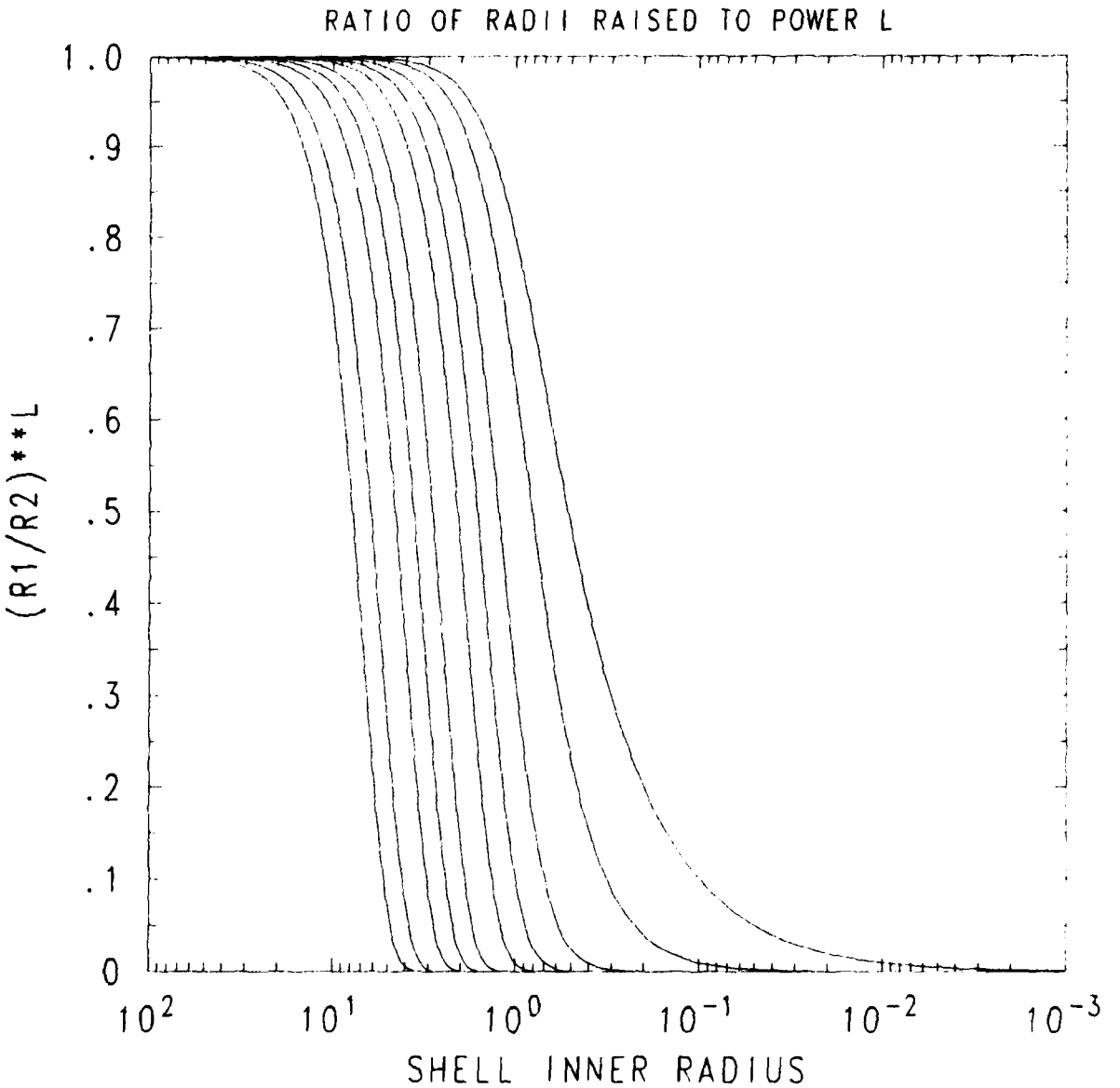

Fig. 2 Ratio $(R_1/R_2)^l$ vs $\log R_1$ for $l = 1, 2, 5, 10, 20, 50, 100, 200, 500, 1000$ (reading from right to left).

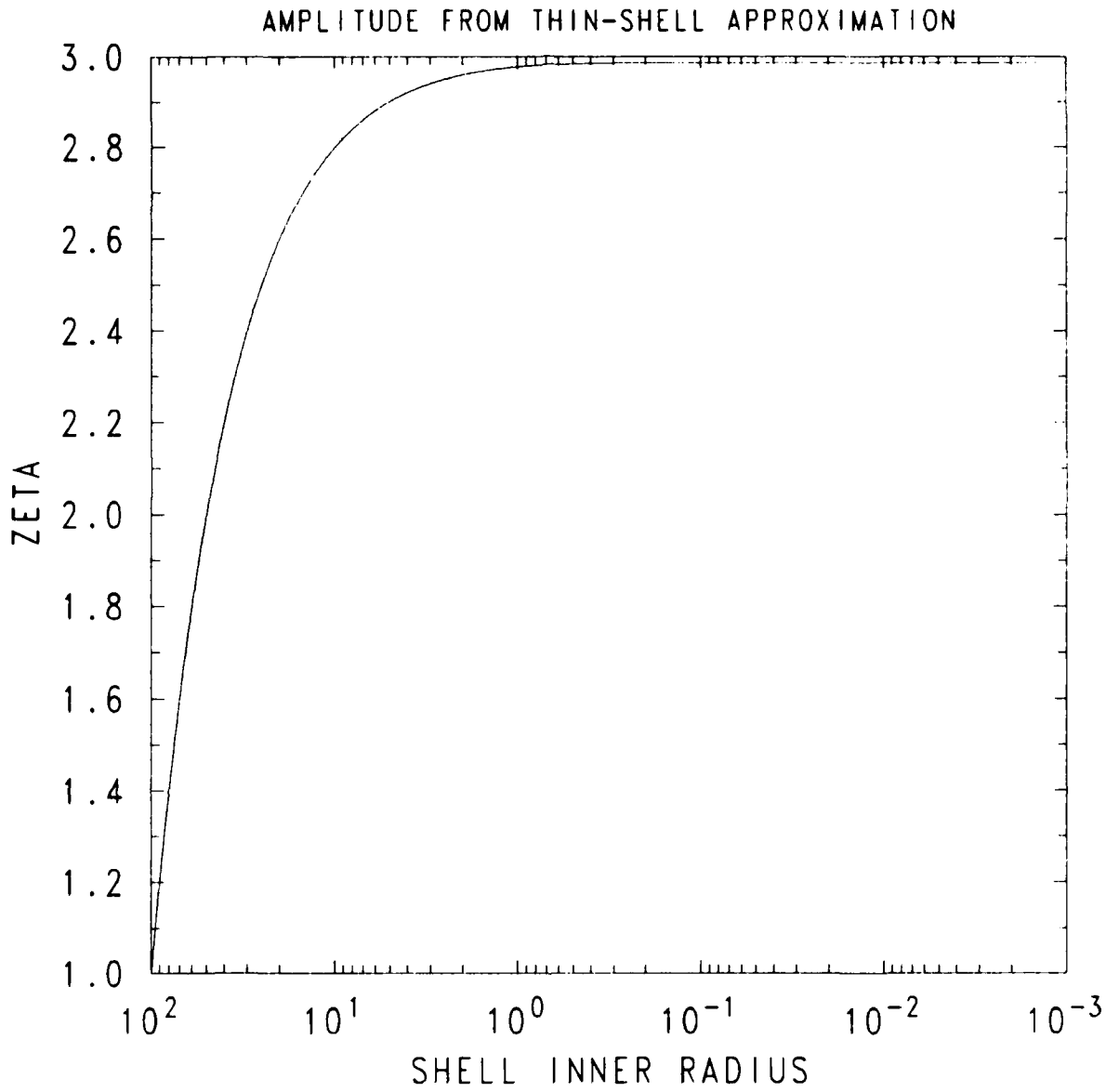

Fig. 3 Linearly increasing amplitude ς_1 (or ς_2) of surface perturbations ς_1, ς_2 vs $\log R_1$ in the thin-shell approximation, assuming initial unit amplitudes and initially vanishing velocity coefficients u_1, u_2.

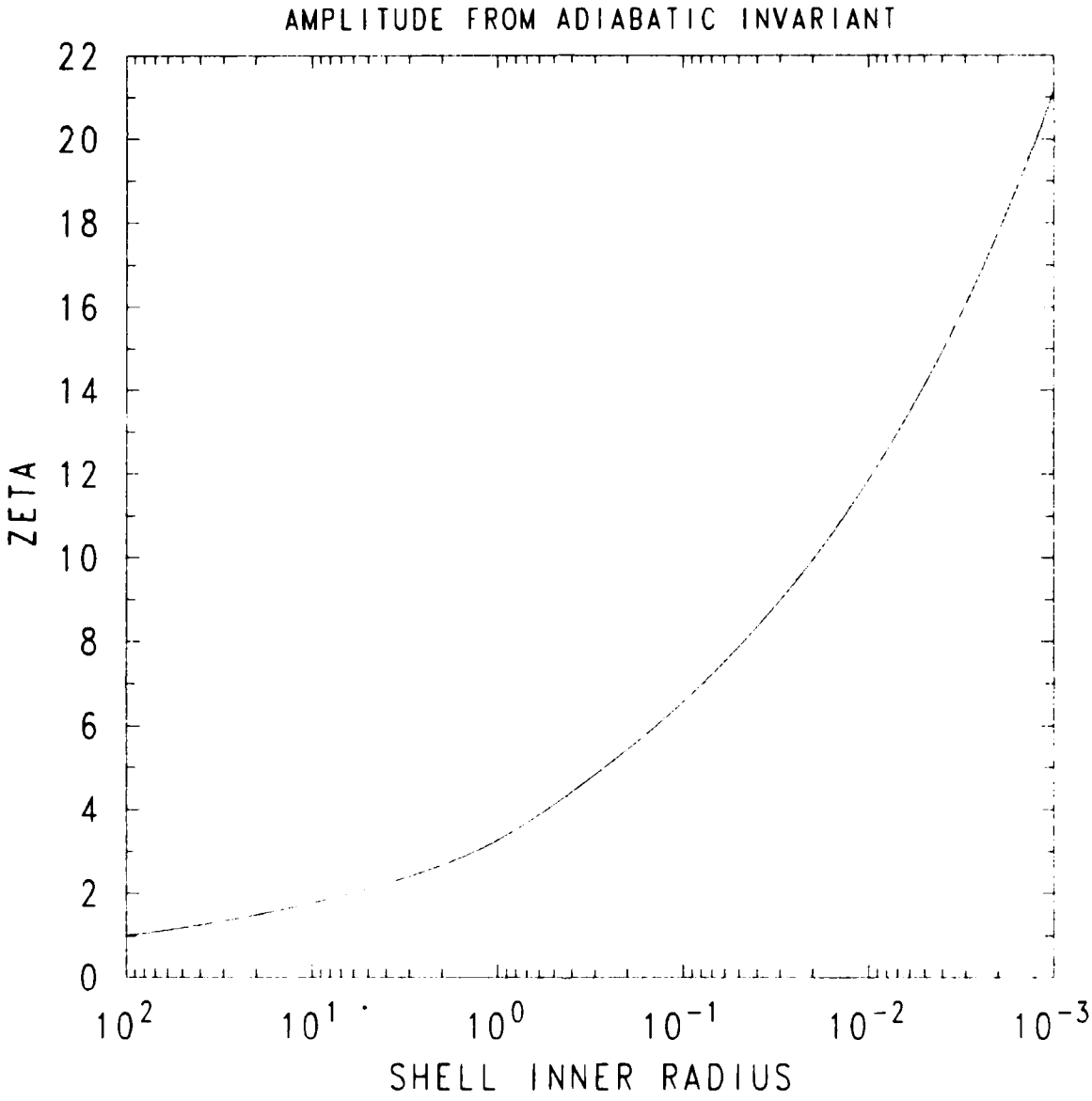

Fig. 4 Amplitude of the inner surface oscillations vs log R_1, obtained from conservation of wave action. The curve has been normalized to have an initial value of unity.

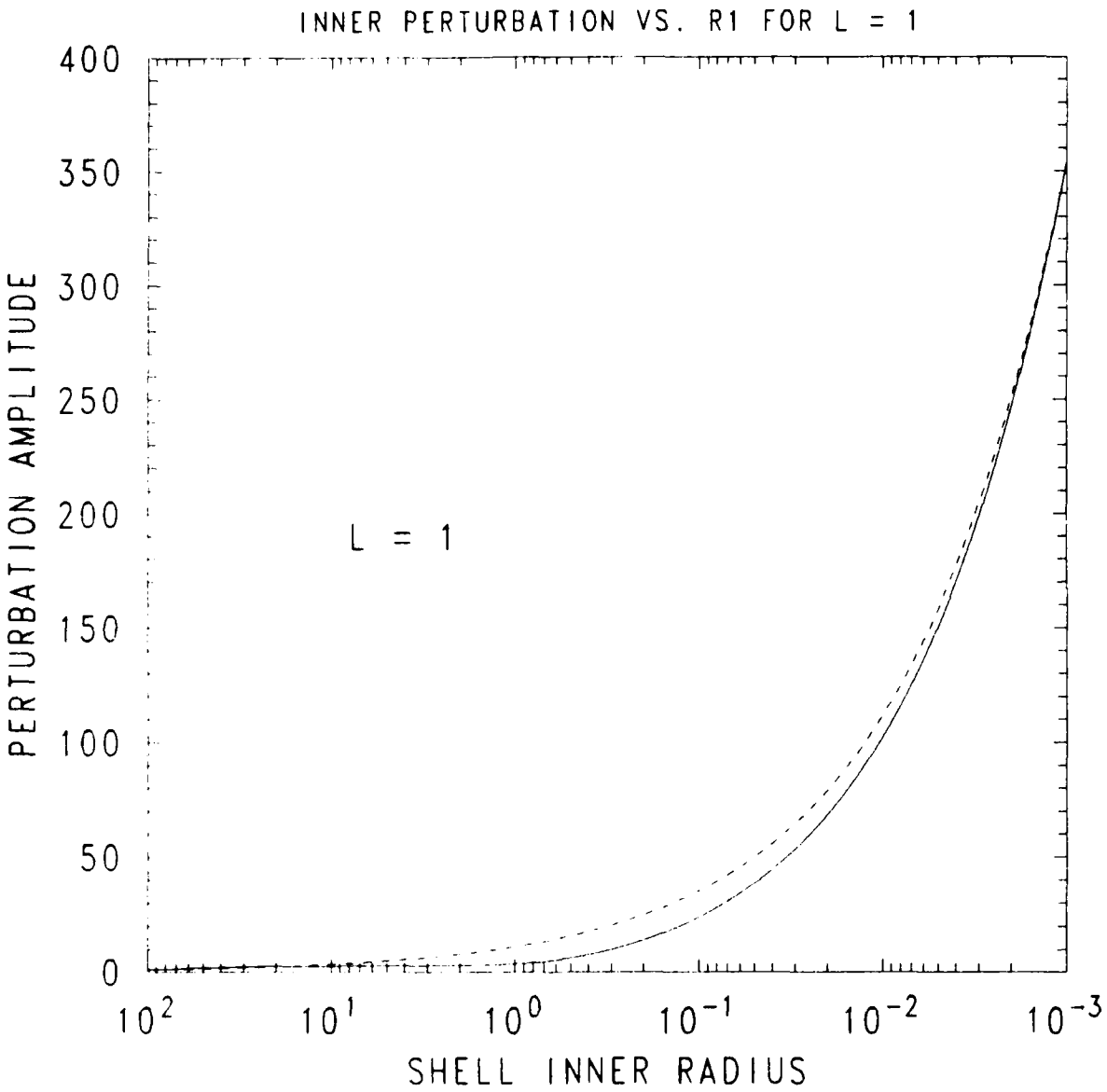

Fig. 5(a) Amplitude of inner surface wave vs log R_1 obtained from numerical solution of the exact equations (21)–(24) for $l = 1$ (solid trace) and as approximated by Eq. (49) (broken trace).

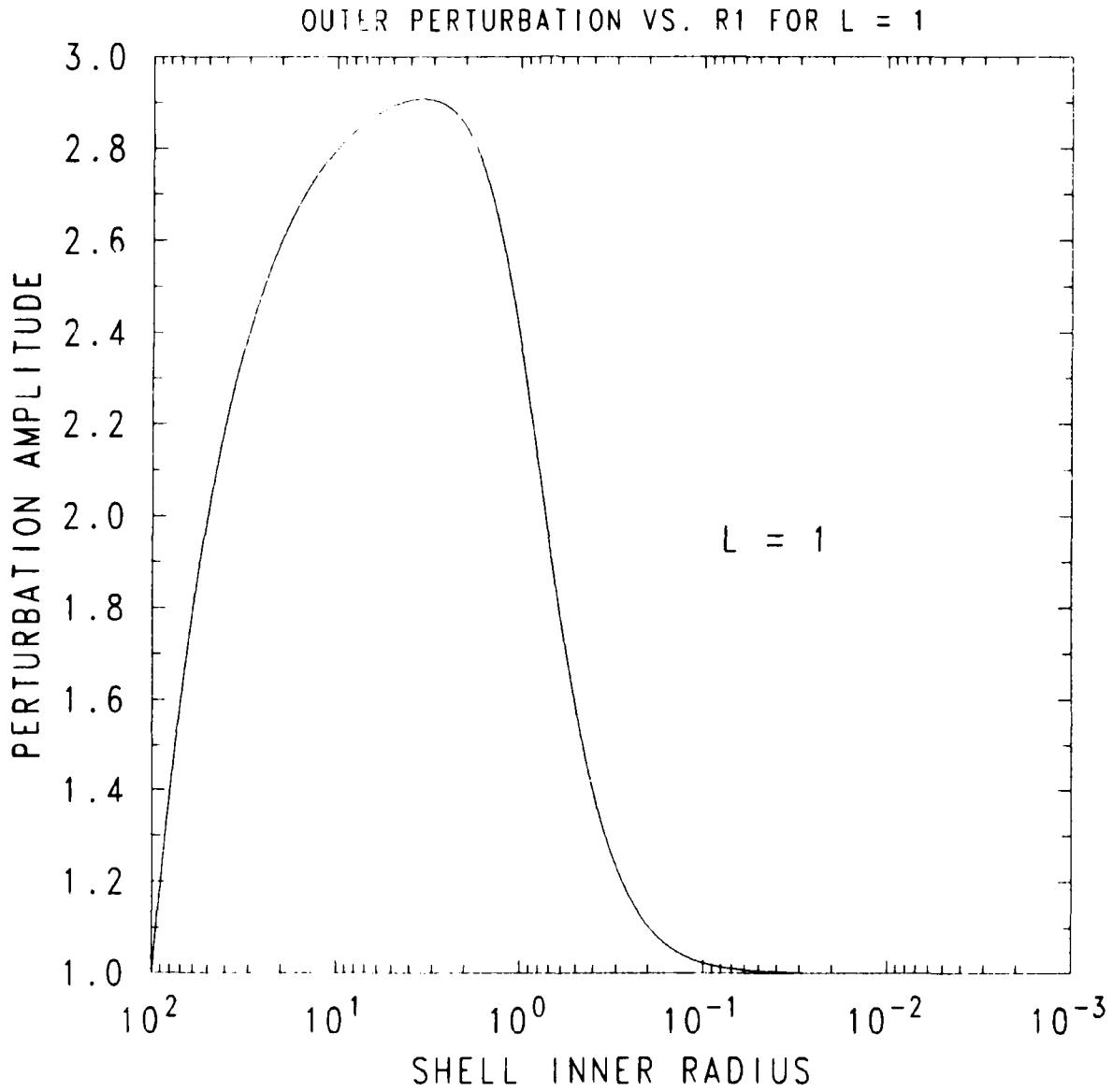

Fig. 5(b) Amplitude of outer surface wave vs log R_1 obtained from numerical solution for $l = 1$.

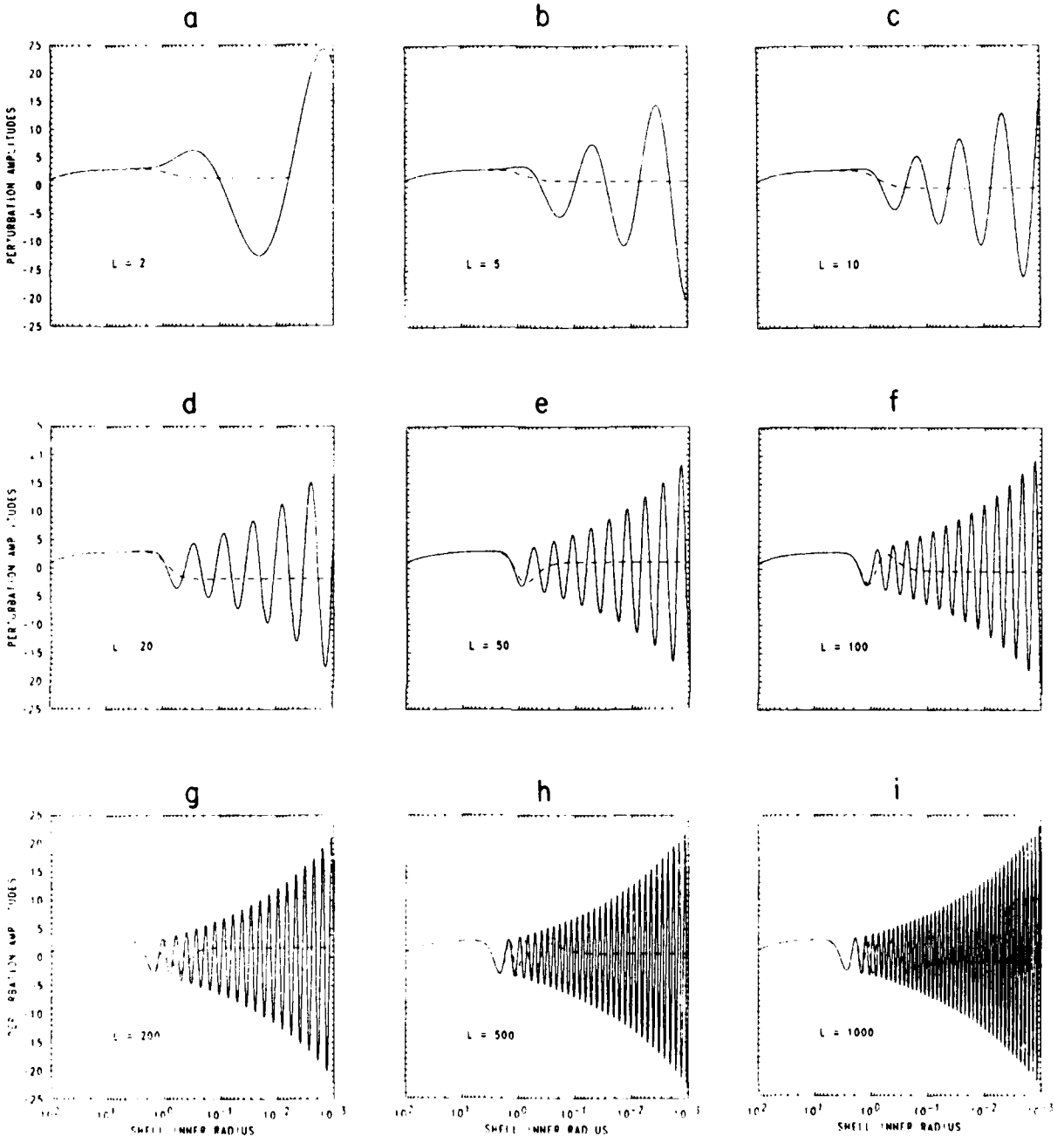

Fig. 6 Amplitudes of inner (solid trace) and outer (broken trace) surface waves vs $\log R_1$ for (a) $l = 2$; (b) $l = 5$; (c) $l = 10$; (d) $l = 20$; (e) $l = 50$; (f) $l = 100$; (g) $l = 200$; (h) $l = 500$; (i) $l = 1000$.

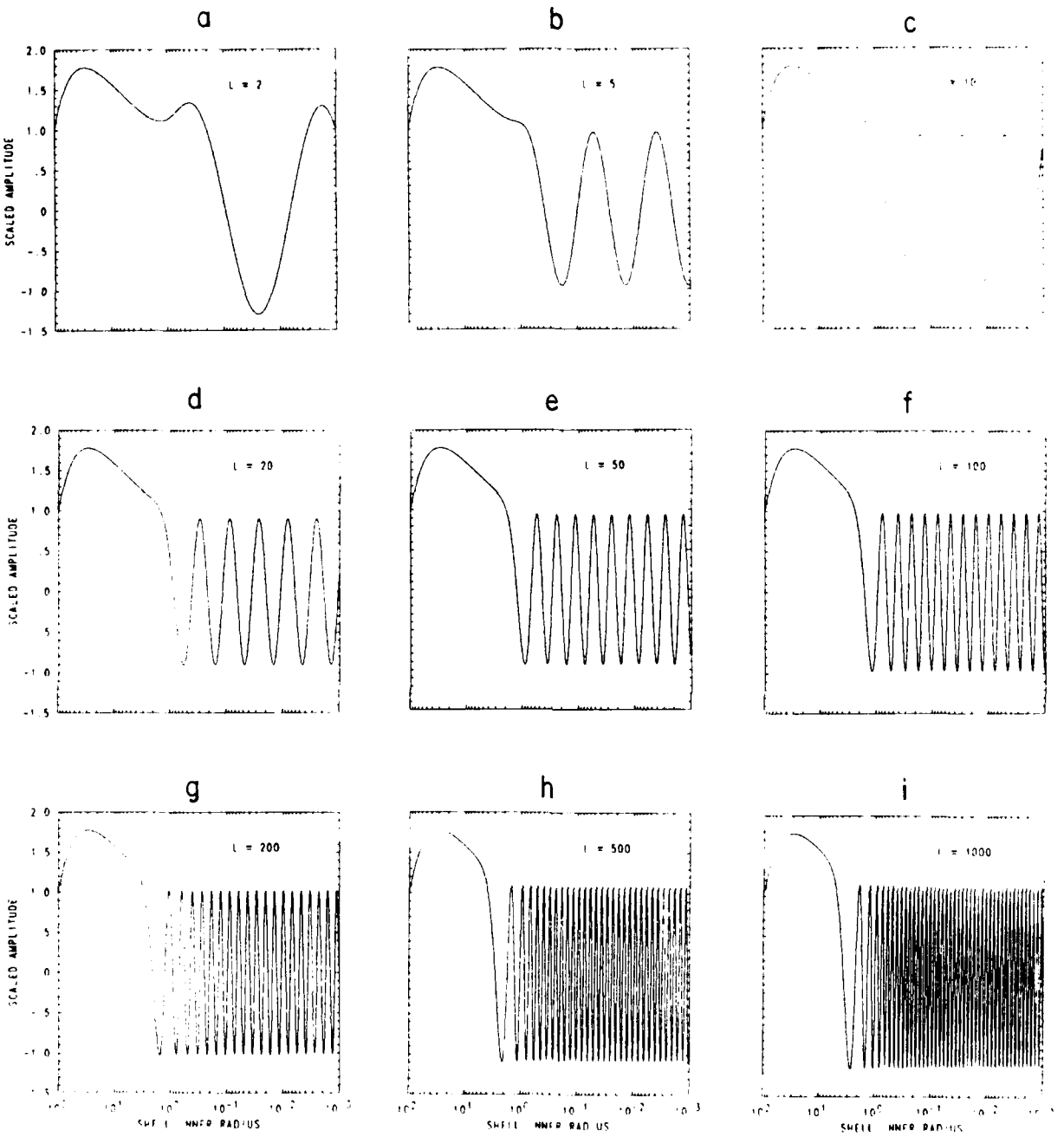

Fig. 7 Amplitudes of inner surface waves shown in Fig. 6, scaled by the approximate function plotted in Fig. 4, vs $\log R_1$ for (a) $l = 2$; (b) $l = 5$; (c) $l = 10$; (d) $l = 20$; (e) $l = 50$; (f) $l = 100$; (g) $l = 200$; (h) $l = 500$; (i) $l = 1000$.

END

2-87

DTIC